Chemical Science

ROYAL SOCIETY OF CHEMISTRY

EDGE ARTICLE

View Article Online
View Journal | View Issue

Cite this: *Chem. Sci.*, 2025, **16**, 16936

All publication charges for this article have been paid for by the Royal Society of Chemistry

Single-walled carbon nanotubes hitchhike on Ly-6C^{hi} monocytes for photoacoustic image-guided photothermal shock therapy of metabolic inflammation

Ruixi Peng,[a] Mengyun He,[a] Yi Yuan,[b] Li-Juan Tang,[a] Jianhui Jiang [a] and Xia Chu *[a]

Received 9th July 2025
Accepted 17th August 2025

DOI: 10.1039/d5sc05091j

rsc.li/chemical-science

Metabolic inflammation (metaflammation) may occur throughout the body and evolve into various metabolic syndromes, so developing a universal approach for diagnosing and treating metaflammation is meaningful. Here, we developed a single-walled carbon nanotube (SWNT)-based photothermal shock therapy (PTST) for photoacoustic image-guided therapy of metaflammation. Mechanistically, SWNTs are specifically taken up by Ly-6C^{hi} monocytes in peripheral blood and then rerouted to inflamed tissues *via* Ly-6C^{hi} monocyte hitchhiking. Due to the accumulation of SWNTs, inflamed tissues can be distinguished by photoacoustic imaging. For treating metaflammation, inflamed tissue gated by photoacoustic imaging is irradiated with near-infrared light and heated to heat shock temperature (around 42 °C). At this temperature, lesional macrophages upregulate the expression of HSP70, which blocks the activation of inflammatory pathways and protects cells from metabolic and inflammatory stress. We successfully identified the lesional liver and aorta and implemented PTST in type 2 diabetes and atherosclerosis model mice. Compared with traditional photothermal therapy (PTT), PTST controls the temperature in a safer and narrower range, implying the prospect of precise temperature control in disease treatment.

Introduction

Metabolic inflammation (metaflammation) is caused by the abnormal activation of immune cells due to the accumulation of excessive nutrients in the blood and organs and is often found in obese individuals.[1–3] Persistent metaflammation is related to the development of severe metabolic syndromes, such as non-alcoholic fatty liver disease (NAFLD),[4] type 2 diabetes (T2D),[5] and atherosclerosis.[6] In fact, organisms possess some mechanisms to combat metabolic stress. Heat shock proteins (HSPs) are a family of stress response proteins found in all species exposed to stressful conditions.[7] Not only does intracellular HSP70 (iHSP70) protect cells from high-temperature damage, but it also exerts a powerful anti-inflammatory effect by blocking the activation of nuclear factor κB (NF-κB) and c-Jun N-terminal kinase (JNK) signal pathways.[8–10] The anti-inflammatory effect of HSP70 protects cells from long- and short-term metabolic challenges in adipose tissue.[11] Unsurprisingly, many metabolic syndrome patients show lower HSP expression.[12–14] Restoring the function of HSPs has been considered an attractive method for preventing and treating metaflammation. Experimental evidence suggests that upregulation of HSPs through transgenosis, HSP70 inducers (BGP-15) or mild hyperthermia can alleviate metaflammation and related diseases in mouse models.[15–18] However, these methods cannot accurately and controllably activate HSPs in inflamed tissues, and undesired activation of HSPs in healthy tissues may result in a series of side effects. Over-expression of HSPs has been proven to be associated with the development of meningitis and cancer, and extracellular HSPs cause a strong inflammatory and immune response.[19–21] Therefore, it is necessary to regulate HSPs at precise time and in specific locations.

Near infrared (NIR) light, characterized by high spatial and temporal resolution, good tissue permeability and minimal photodamage, has emerged as a powerful tool for manipulating cell behavior.[22] Together with photosensitive nanomaterials, more diverse functions can be achieved within cells under the control of NIR light. For example, thermosensitive promoters, thermosensitive cation channel proteins and lipid rafts can be controlled by the photothermal effect of nanomaterials.[23–27] However, targeted delivery of nanomaterials to specific organs and cells still faces huge challenges. In particular, metaflammation occurs in multiple sites of the body, including the vasculature, heart, kidney, brain, pancreatic islet, skeletal muscle and liver.[5] To solve this problem, we turned our

[a]*State Key Laboratory of Chemo and Biosensing, College of Chemistry and Chemical Engineering, Hunan University, Changsha 410082, P. R. China. E-mail: xiachu@hnu.edu.cn*

[b]*Chongqing Materials Research Institute Co., Ltd, Chongqing 400707, P. R. China*

attention to single-walled carbon nanotubes (SWNTs), because they can be specifically and rapidly taken up by Ly-6C^{hi} monocytes in blood.[28] These cells, being the primary circulating cells, are rapidly recruited to inflamed tissues, differentiating into inflammatory macrophages and playing a crucial role in the inflammation process.[29] Therefore, we reasoned that SWNTs can accumulate in macrophages within inflamed tissue *via* Ly-6C^{hi} monocyte hitchhiking. Moreover, SWNTs possess excellent optical absorption in the NIR region, high photothermal conversion efficiency and good biocompatibility, which are suitable for controlling cells *via* NIR light *in vivo*. Furthermore, irradiation of SWNTs with NIR generates a strong photoacoustic (PA) signal.[30,31] PA imaging, which combines the superior sensitivity of optical imaging with the sufficient penetration depth of acoustic imaging, is suitable for noninvasive imaging with deep tissue penetration and high spatial resolution.[32,33] Accordingly, SWNTs are promising for identifying inflamed tissues and enabling PA image-guided therapy for metaflammation.

In this study, we proposed a new strategy to alleviate metaflammation by photothermal regulation of HSP70 in lesional macrophages, which was named photothermal shock therapy (PTST). The mechanism of PTST is shown in Fig. 1. Once the SWNTs are injected intravenously, they are rapidly and specifically engulfed by Ly-6C^{hi} monocytes and rerouted to inflamed tissue *via* Ly-6C^{hi} monocyte hitchhiking. Then, PA imaging is used for finding the accurate lesional site and for gating the location of NIR irradiation. After being exposed to NIR laser irradiation, the macrophages located in inflamed tissues upregulate the expression of HSP70 in response to the subsequent temperature rise. Unlike traditional photothermal therapy (PTT) that requires heating tissue to more than 60 °C, PTST only needs to heat cells to around 42 °C, which is safe and sufficient to induce the expression of HSP70. HSP70 blocks the activation of NF-κB and JNK inflammatory pathways and the secretion of inflammatory cytokines, as well as protects cells under inflammatory conditions. We demonstrated that SWNTs were taken up by almost 100% of Ly-6C^{hi} monocytes in peripheral blood and 40% of macrophages in the inflamed liver and aorta. Due to the different accumulation tendencies of SWNTs, healthy and pathological tissues can be effectively distinguished by PA imaging. We successfully implemented PTST in *db*/*db* mice (T2D model mice) and *ApoE*$^{-/-}$ mice (atherosclerosis model mice). After a period of PTST, the symptoms of both model mice were alleviated. We believe that PTST opens up new horizons for traditional PTT, and the customized delivery of heat signals to cells enables PTT to evolve into more diverse applications.

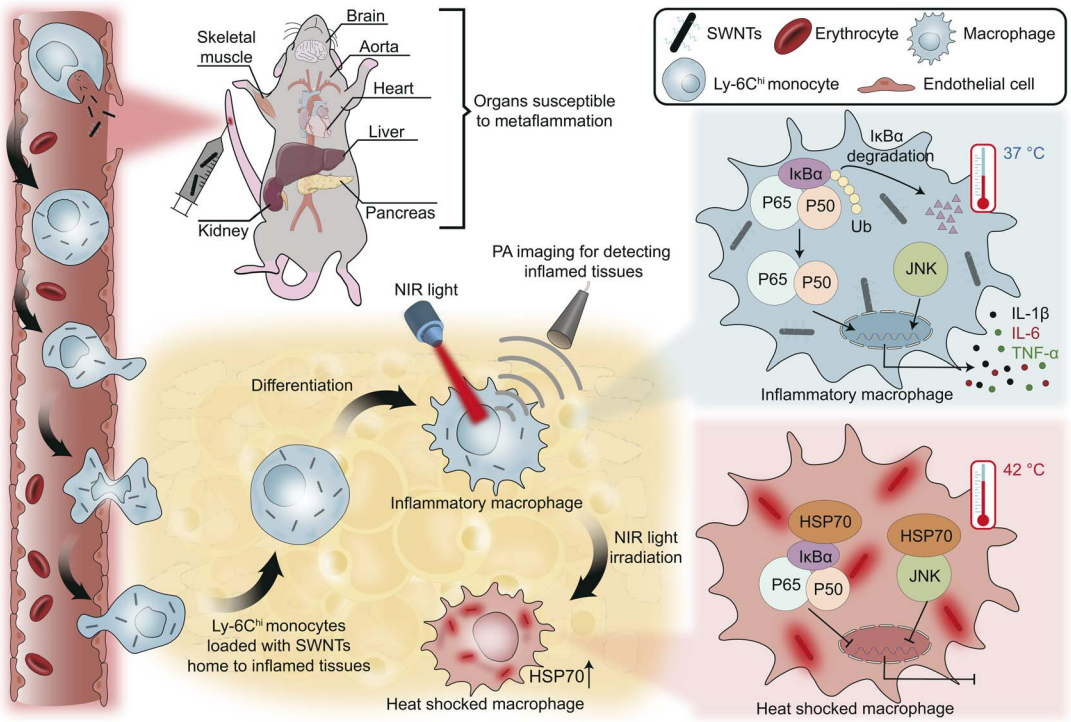

Fig. 1 Schematic illustration depicting the accumulation of SWNTs in lesional macrophages and the mechanism by which PTST alleviates inflammation. Metaflammation may occur throughout the body, including the vasculature, heart, kidney, brain, pancreatic islet, skeletal muscle and liver. For targeting inflamed tissues, SWNTs are injected *via* the tail vein, and they are rapidly and specifically taken up by Ly-6C^{hi} monocytes in the blood. The Ly-6C^{hi} monocytes then carry SWNTs to the lesional sites and differentiate into macrophages. PA imaging is used to identify the location of SWNT accumulation. At physiological temperature (37 °C), NF-κB and JNK inflammatory pathways of lesional macrophages are abnormally and constantly activated, leading to the continuous secretion of pro-inflammatory factors (IL-6, IL-1β and TNF-α) and the development of chronic inflammation. After 808 nm laser irradiation, the temperature of lesional macrophages increases to around 42 °C, causing the upregulation of HSP70 in lesional macrophages. HSP70 protects IKBα from degradation, inhibits the phosphorylation of P65 and JNK and thereby suppresses the activation of NF-κB and JNK signal pathways.

Results and discussion

Preparation and characterization of SWNTs

The synthesis of SWNTs was performed as previously described.[34] Raw SWNTs were functionalized with 1,2-distearoyl-*sn*-glycero-3-phosphoethanolamine-*N*-(polyethylene glycol)-5000 (DSPE-PEG_{5000}) through hydrophobic interaction. This non-covalent method is more efficient and does not affect the inherent optical properties of SWNTs.[35] DSPE-PEG_{5000} is used to disperse SWNTs in aqueous solutions, prolong *in vivo* circulation time and enhance biocompatibility. As shown by transmission electron microscopy (TEM) and atomic force microscopy (AFM) images, SWNTs exhibited a 2–3 nm nanotube structure (Fig. S1A and B). The UV-vis-NIR spectra show that SWNTs have strong absorption in the NIR region (Fig. S1C). Raman spectra show that SWNTs possess three characteristic peaks, a strong G band near 1580 cm^{-1}, a D band near 1360 cm^{-1} and a radial breathing mode (RBM band) around 250 cm^{-1} (Fig. S1D). The G band represents the tangential displacement of carbon atoms, the D band is derived from carbon tube defects and the RBM band is the signature vibration of one-dimensional nanostructures. The PA spectra demonstrated that SWNTs can generate strong PA signals at 700–900 nm (Fig. S2), and the PA intensity is highly dependent on the concentration of SWNTs (Fig. 2A). SWNTs remained stable for 7 days in ddH_2O, PBS, fetal bovine serum (FBS) and complete medium, suggesting good stability and dispersibility of SWNTs in various solution systems (Fig. S3).

Optimization of the irradiation strategy

As temperatures increased to 42 °C, cells were subjected to heat shock and subsequently upregulated the expression of HSP70. Incubation at this temperature for several hours does not significantly affect the activity of cells, while cells incubated above 46 °C will die within a few minutes.[36] So it is necessary to stabilize the photothermal temperature at about 42 °C. In order to find suitable irradiation conditions to implement PTST, we evaluated the photothermal effect of SWNTs. SWNTs dissolved in PBS were irradiated with an 808 nm laser for 5 min. The rate of temperature rise increased with the increase of SWNT concentration (0–200 μg mL^{-1}) or laser power density (0.1–1.0 W cm^{-2}) (Fig. S4). At a relatively low SWNT concentration (50 μg mL^{-1}) and laser power density (0.5 W cm^{-2}), the temperature reached 42 °C in 2 min and tended to be stable when it rose to 47 °C (Fig. S4B). We adopted this condition and further adjusted the irradiation strategy for maintaining the photothermal temperature at about 42 °C. As shown in Fig. 2C, we adopted a discontinuous irradiating mode that repeated the

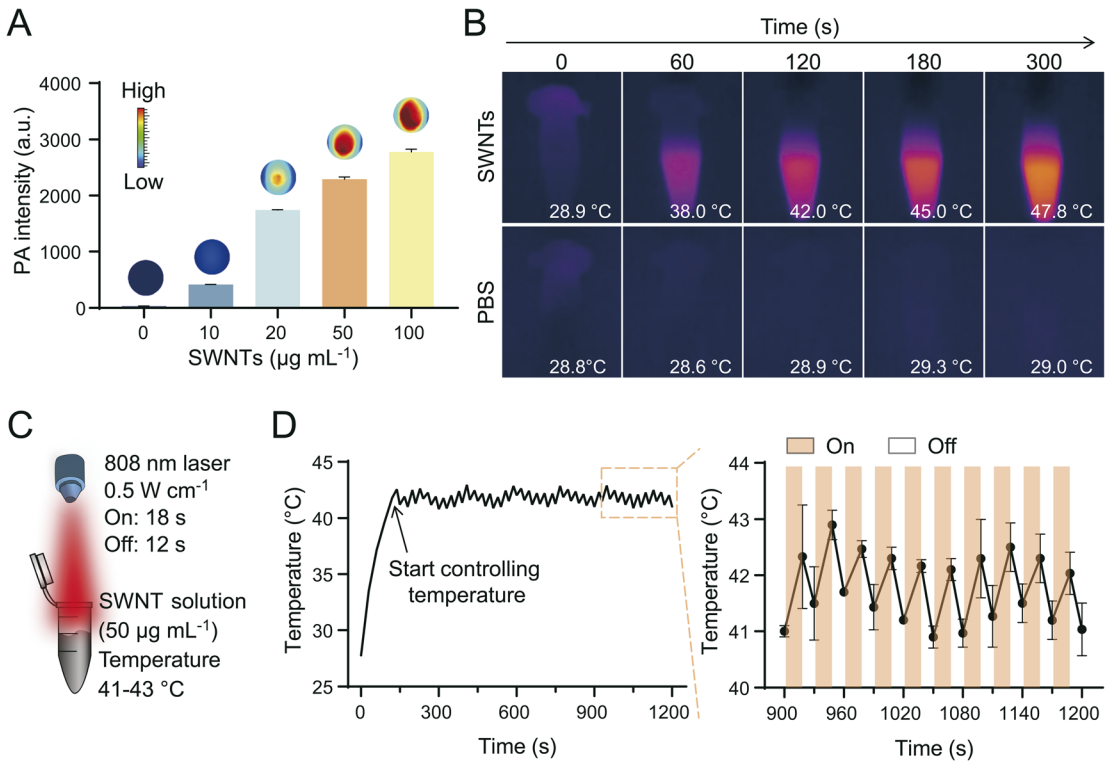

Fig. 2 Photothermal and photoacoustic effects of SWNTs. (A) PA intensity and imaging of SWNTs dispersed in PBS buffers with different concentrations (0, 10, 20, 50, and 100 μg mL^{-1}). (B) Real-time infrared thermal imaging of SWNTs (50 μg mL^{-1}) and PBS with NIR irradiation (808 nm, 0.5 W cm^{-2}). (C) Schematic illustration of the irradiation strategy. SWNTs (50 μg mL^{-1}) were irradiated with NIR (808 nm, 0.5 W cm^{-2}). Once the temperature reached 42 °C, adjust the irradiation strategy (On: 18 s, Off: 12 s) to stabilize the temperature. (D) Transient thermal measurements of SWNTs (50 μg mL^{-1}) under precisely controlled NIR (808 nm, 0.5 W cm^{-2}) irradiation. The picture on the right is an enlarged view of the last 5 min of the left image. Yellow areas indicate irradiation, while white areas do not. All experiments were repeated three times, and data are presented as mean ± S.D.

cycle of turning on the laser for 18 s and then turning off for 12 s once the photothermal temperature reached 42 °C. Discontinuous heating mode has been proven to be more effective in inducing HSPs and conducive to heat diffusion, which avoids local overheating.[37] Under this irradiation strategy, the photothermal temperature was kept between 41 and 43 °C for a long time (Fig. 2D). In summary, we could easily and accurately control the photothermal temperature by adjusting the concentration of SWNTs, the laser power density and the irradiation strategy, which laid the foundation for us to test PTST *in vivo* and *in vitro*.

Cytotoxicity assay of PTST

Good biocompatibility and low toxicity are prerequisites for applying PTST. Thus, we used the Cell Counting Kit-8 (CCK-8) assay to examine the toxicity of SWNTs and heat shock temperature on mouse leukemia monocyte macrophage RAW264.7 cells. The viability data of RAW264.7 incubated with SWNTs (0–200 μg mL^{-1}) for 24 hours showed no obvious cytotoxicity, indicating their good biocompatibility (Fig. S5A). To assess the cytotoxicity of PTST on macrophages, RAW264.7 cells were incubated with SWNTs (50 μg mL^{-1}) for 2 hours and then exposed to NIR (808 nm, 0.5 W cm^{-2}) laser irradiation. By precisely controlling irradiation conditions, RAW264.7 cells were subjected to heat shock temperature for different times (0–25 min). Similarly, no obvious cytotoxicity was observed, indicating that RAW264.7 cells are tolerant to this temperature (Fig. S5B). These data confirmed that PTST can be achieved safely and conveniently by using SWNTs and NIR light.

Some evidence indicates that monocytes secrete IL-1β after phagocytosing multi-walled carbon nanotubes (MWCNTs), triggering an inflammatory response.[38] Therefore, we further tested whether SWNTs could stimulate RAW264.7 cells to secrete IL-1β. ELISA data showed that RAW264.7 cells co-incubated with SWNTs (50 μg mL^{-1}) for 6 hours did not upregulate the expression of IL-1β (Fig. S6).

Upregulating HSP70 and inhibiting inflammatory pathways by PTST *in vitro*

We first verified whether PTST could upregulate HSP70 in RAW264.7 cells. RAW264.7 cells were co-incubated with SWNTs (50 μg mL^{-1}) for 2 hours and then exposed to NIR (808 nm, 0.5 W cm^{-2}) laser irradiation for different times (Fig. 3A). We also placed RAW264.7 cells in a 42 °C water bath for 1 hour as a positive control. The western blot data showed that the expression of HSP70 was significantly increased by only 5 min of

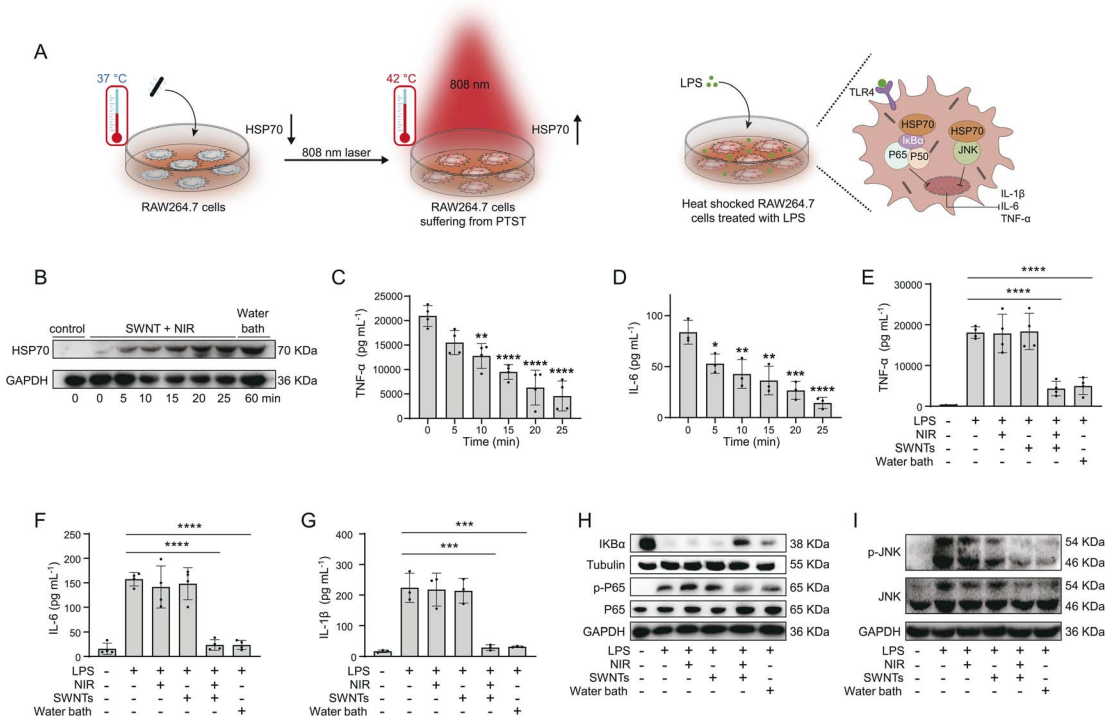

Fig. 3 PTST upregulates the expression of HSP70 and inhibits the activation of inflammatory pathways. (A) Schematic diagram of RAW264.7 cells receiving PTST treatment and inflammatory pathway activation after LPS stimulation. (B) Western blot analysis of the expression of HSP70 in RAW264.7 after different times of PTST. The control group received no treatment. The group treated in a water bath (42 °C) for 1 hour served as the positive control. GAPDH was used as a loading control. (C and D) ELISA analysis of the secretion of TNF-α (C) and IL-6 (D) by RAW264.7 cells pretreated with PTST at different times after LPS stimulation. Data are shown as mean ± S.D. of three or four independent experiments, and analyzed by one-way ANOVA. *$p \leq 0.05$, **$p \leq 0.01$, ***$p \leq 0.001$, ****$p \leq 0.0001$ *vs.* 0 min. (E–G) ELISA analysis of the secretion of IL-6 (E), TNF-α (F) and IL-1β (G) by RAW264.7 cells after the indicated treatment. The group treated in a water bath for 1 hour served as the positive control. Data are shown as mean ± S.D. of three or four independent experiments, and analyzed by one-way ANOVA. ***$p \leq 0.001$ and ****$p \leq 0.0001$. (H and I) Western blot analysis of the expression of IKBα and phosphorylation of p65 (H) and JNK (I) in RAW264.7 cells after the indicated treatment. The group treated in a water bath for 1 hour served as the positive control. Tubulin and GAPDH were used as a loading control.

PTST and the expression of HSP70 by 25 min of PTST was similar to that of the positive control (Fig. 3B). Because extracellular HSP70 (eHSP70) served as a potent proinflammatory signal, we next sought to explore whether PTST could promote RAW264.7 cells releasing HSP70 out of cells. We collected the supernatant of RAW264.7 cells treated with PTST and found that the level of HSP70 was equivalent to that of the untreated group (Fig. S7). The eHSP70 was also unchanged in groups treated separately with SWNTs or NIR. These data proved that PTST was a powerful way to induce iHSP70 but not eHSP70.

Macrophages treated with LPS can be polarized to the M1 phenotype (inflammatory phenotype), which is commonly used in establishing an inflammation model. We used LPS to stimulate the PTST-treated RAW264.7 cells and characterized their secretion of inflammatory factors (Fig. 3A). As shown in Fig. 3C and D, the secretion of IL-6 and TNF-α decreased with the prolongation of PTST pretreatment time, and 5 min of PTST could be effective. This trend was contrary to the expression of iHSP70: the more HSP70 expressed by RAW264.7 cells, fewer pro-inflammatory factors they secreted after LPS treatment. The decline of IL-1β, IL-6 and TNF-α secreted by RAW264.7 cells treated in a 42 °C water bath was comparable to that of RAW264.7 cells treated with 25 min PTST, while RAW264.7 cells treated only with SWNTs or NIR had no inhibitory effect on the secretion of inflammatory factors (Fig. 3E–G). We further investigated the impact of PTST on the macrophage inflammatory pathway. The activation of the NF-κB pathway is characterized by the degradation of IKBα as well as the phosphorylation of P65. The activation of JNK is featured by phosphorylation of JNK. As shown in Fig. 3I and J, degradation of IKBα as well as phosphorylation of p65 and JNK was found in LPS-treated RAW264.7 cells, while cells pretreated with PTST or in a water bath suppressed the activation of these inflammatory pathways. RAW264.7 cells treated with SWNTs or NIR alone did not affect the activation of these two pathways (Fig. 3H and I). To sum up, PTST could inhibit the secretion of inflammatory factors and the activation of inflammatory pathways in cells exposed to inflammatory stimulation.

SWNTs are selectively taken up by inflammatory monocytes

To investigate the interaction between SWNTs and monocytes, SWNTs were labeled with FITC or Cy5.5 (SWNT-FITC and SWNT-Cy5.5). We first studied the interaction between RAW264.7 cells and SWNTs *in vitro*. SWNT-FITC or SWNT-Cy5.5 were significantly taken up by RAW264.7 cells within 0.5 h, and the uptake of SWNTs increased gradually with the extension of co-incubation time (Fig. S8A and B). These data demonstrated that the uptake of SWNTs by monocytes was very fast. We next explored which cell types were prone to uptake SWNTs in peripheral blood. Blood from wild type (WT) C57BL/6 mice was collected after 2 hours of tail vein injection of SWNT-FITC.

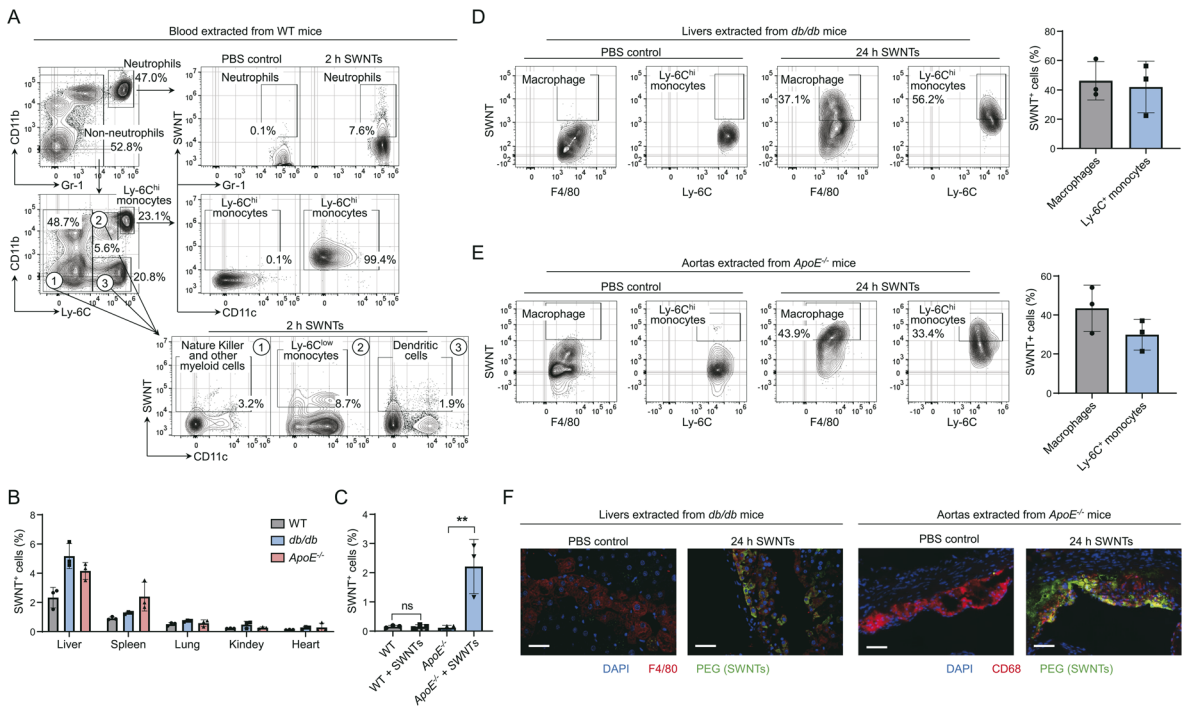

Fig. 4 SWNTs were selectively taken up by inflammatory monocytes and accumulated in inflammatory tissues. (A) Flow cytometry assay to identify the selective uptake of SWNTs into white blood cells. $n = 3$ mice per group. (B) Flow cytometry analyses of homogenized organs confirmed the trend of uptake by organs in WT, *db*/*db* and *ApoE*$^{-/-}$ mice. $n = 3$ mice per group. (C) Flow cytometry analyses of homogenized aorta confirmed the selective accumulation of SWNTs in the lesional aorta. $n = 3$ mice per group. (D and E) SWNTs accumulated within macrophages and Ly-6C^{hi} monocytes in the lesional liver of *db*/*db* mice (D) and aorta of *ApoE*$^{-/-}$ mice (E). (F) Lesional macrophage and SWNT co-localization was confirmed by confocal images of the liver of *db*/*db* mice and aortic sinus of *ApoE*$^{-/-}$ mice. Blue: nucleus, red: macrophage and green: SWNTs. Scale bar: 50 μm. $n = 3$ mice per group. All data are presented as mean ± S.D. All statistical analysis was conducted using one-way ANOVA. $^{**}p \leq 0.01$ and ns, no significance.

Fluorescence activating cell sorter (FACS) analysis was used to identify the subsets of immune cells that took up SWNTs in blood. Near 100% of circulating Ly-6C^{hi}, CD11b^{+} monocytes took up SWNTs (Fig. 4A). However, other circulating white blood cells exhibited minimal uptake of SWNTs, such as 7.6% of neutrophils, 8.7% of Ly-6C^{low} monocytes and 1.9% of dendritic cells (Fig. 4A). These data indicated that SWNTs are quickly and selectively taken up by Ly-6C^{hi} monocytes once they are injected into blood.

SWNTs accumulate in inflamed tissues

Because Ly-6C^{hi} monocytes are recruited to inflamed tissues, we further explored whether SWNTs could accumulate in lesional tissues *via* Ly-6C^{hi} monocyte hitchhiking. *ApoE*$^{-/-}$ mice are generally used to study atherosclerosis, and their aortic arches suffer from chronic inflammation.[39,40] *db*/*db* mice are typical T2D model mice and their livers, the main insulin-sensitive organ, are affected by chronic inflammation.[41] *ApoE*$^{-/-}$, *db*/*db* and WT mice were used for the following experiments. After systemic injection of SWNTs for 24 hours, flow cytometry analyses of the homogenized organs showed that high uptake of SWNTs in macrophage-rich organs (liver and spleen) in all three model mice (Fig. 4B and S9). Moreover, the percentage of cells engulfing SWNTs in the liver of *db*/*db* mice was twice that of WT mice (Fig. 4B and S9A and B). In the aorta of *ApoE*$^{-/-}$ mice, more than 2% of cells took up SWNTs, while negligible cells in the aorta of WT mice took up SWNTs (Fig. 4C and S10). These data indicated that inflamed tissues accumulated more SWNTs. We further explored which cell type in inflamed tissues carried SWNTs. In the lesional liver and aorta, around 40% of Ly-6C^{hi} monocytes and macrophages took up SWNTs (Fig. 4D and E), while below 10% of other types of cells took up SWNTs (Fig. S11). Confocal microscopy also showed that SWNTs co-localized with macrophages in lesional tissues (Fig. 4F). Therefore, we inferred that the majority of SWNTs accumulated in the lesional macrophages.

Due to the different accumulation patterns of SWNTs in healthy and lesional tissues, we next explored whether this difference could be distinguished through PA imaging to help us identify inflammatory sites. The PA signal in the liver of *db*/*db* mice increased rapidly and reached its peak 4 hours after injection of SWNTs. The PA signal change in the liver of WT mice displayed the same trend, but the signal intensity was twice weaker than that of the liver in *db*/*db* mice (Fig. 5A). The PA signal observed in the liver of WT mice arises from the fact that the liver serves as the primary organ for nanomaterial clearance. In contrast, the inflamed liver not only clears SWNTs but also attracts a significant number of Ly-6C^{hi} monocytes, thereby accounting for the intensified PA signal detected in the inflamed tissue. Therefore, SWNTs can effectively distinguish between a healthy liver and an inflamed liver. The carotid artery of *ApoE*$^{-/-}$ mice displayed the strongest PA signal (about 7 times higher than before injection of SWNTs) after 12 hours of injection of SWNTs, while the carotid artery of WT mice could not detect a PA signal change after injection of SWNTs (Fig. 5B). Thus, SWNTs can also effectively distinguish between a healthy aorta and an inflamed aorta. The above data proved that SWNTs served as a universal PA contrast agent for detecting tissues affected by metaflammation. We also used an *in vivo* image

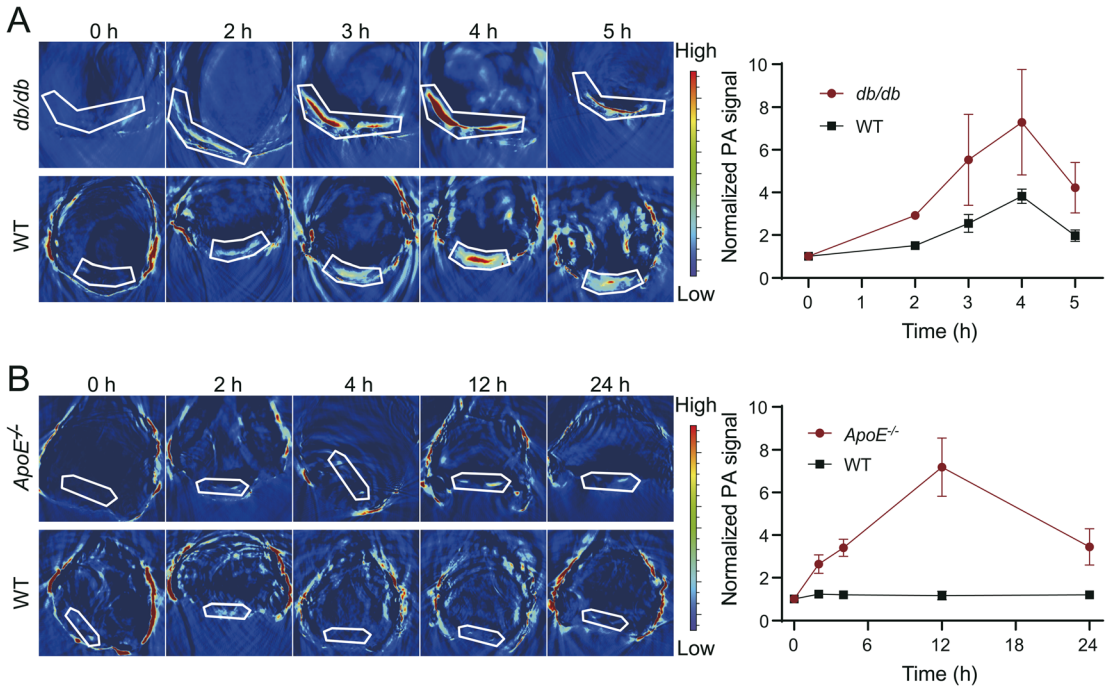

Fig. 5 *In vivo* photoacoustic imaging of SWNTs. (A and B) Typical cross-section and side-looking photoacoustic photos of the liver (A) and aorta (B) with different time periods after injection of SWNTs into *ApoE*$^{-/-}$, *db*/*db* and WT mice. $n = 3$ mice per group. The areas within the white line were used to indicate liver or carotid artery locations. PA intensity of the carotid artery or liver at different time points is shown on the right. All data are presented as mean ± S.D.

system (IVIS) to monitor the real-time distribution of SWNT-Cy5.5 *in vivo*. The liver fluorescence of *db*/*db* mice reached its peak 4 hours post-injection of SWNT-Cy5.5, which was much higher than that of WT mice (Fig. S12). The fluorescence in the aorta site of *ApoE*$^{-/-}$ mice reached its peak 12 hours post-injection of SWNT-Cy5.5, while WT mice had negligible fluorescence in the aorta site (Fig. S13). The trend of the fluorescence signal was similar to the PA signal.

In order to achieve PTST *in vivo*, we explored whether SWNTs accumulated in organs could induce sufficient temperature rise after NIR irradiation. Organs from WT mice were collected 12 hours after injection of SWNTs and received NIR (808 nm, 0.5 W cm^{-2}) irradiation for 5 min. Only the temperature of the liver could rise to 46 °C after 5 min of irradiation, while the temperatures of other organs did not exceed 40 °C (Fig. S14A–G). Livers of *db*/*db* mice were collected 4 hours after injection of SWNTs and received NIR (808 nm, 0.5 W cm^{-2}) irradiation for 5 min and the temperature could reach nearly 50 °C (Fig. S14H–J). Aortas of *ApoE*$^{-/-}$ mice were collected 12 hours after injection of SWNTs and received NIR (808 nm, 0.5 W cm^{-2}) irradiation for 5 min and the temperature could reach nearly 45 °C (Fig. S14K–M). The temperature of organs collected from the PBS group was almost unchanged after NIR irradiation (Fig. S14). Fundamentally, the trend of temperature rise was consistent with the amount of SWNTs accumulated in organs (Fig. 4B and C). These data implied that SWNTs accumulated in inflamed tissues were sufficient for implementing PTST.

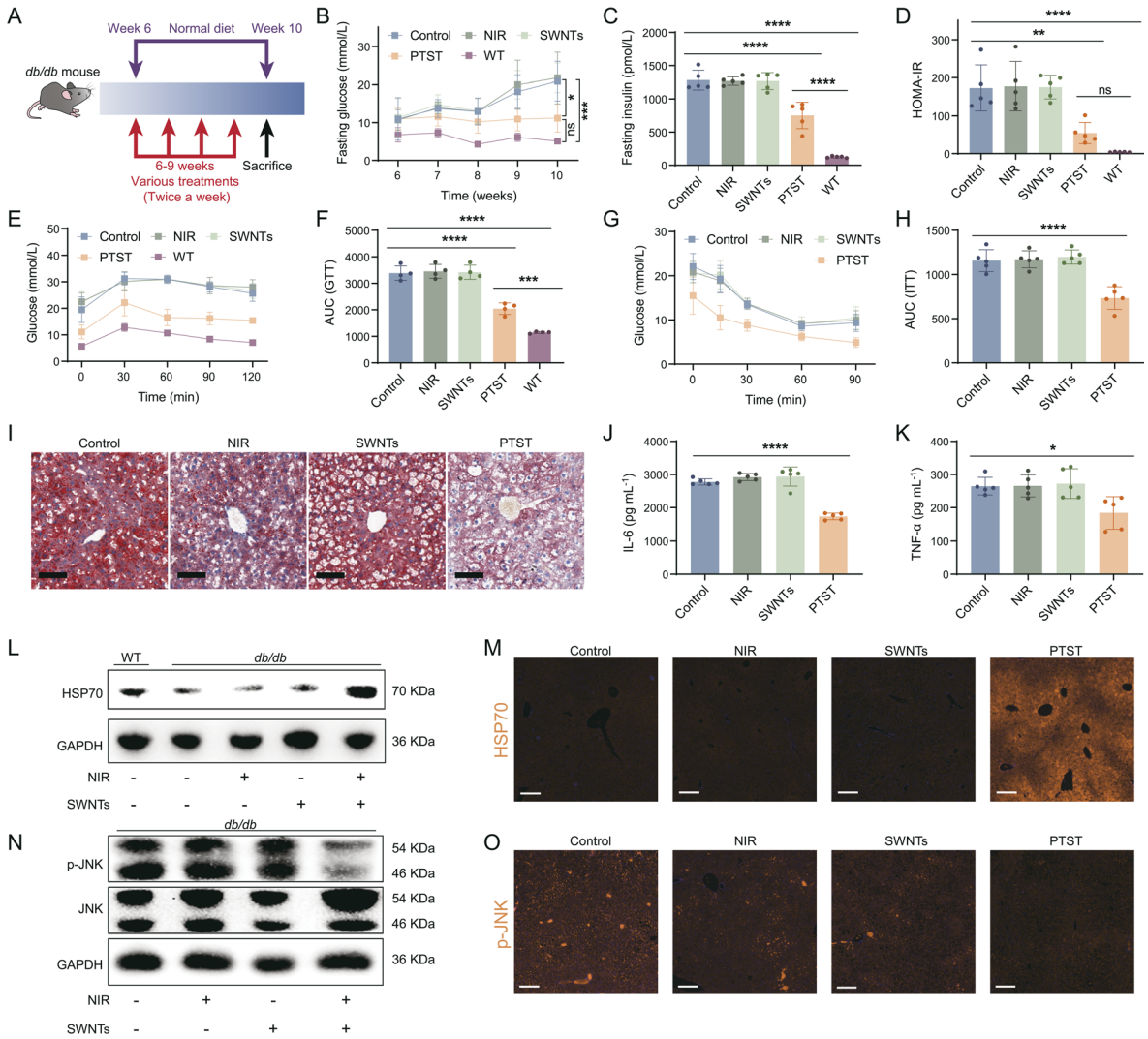

Fig. 6 *In vivo* PTST relieved T2D. (A) Schematic illustration of *db*/*db* mice receiving various treatments. (B) Fasting blood glucose concentrations of each group measured weekly ($n = 5$). (C) Fasting insulin value of mice at the age of 10 weeks ($n = 5$). (D) HOMA-IR value of mice at the age of 10 weeks ($n = 5$). (E and F) Blood glucose levels during IPGTTs and quantification of the area under the curve (AUC, $n = 4$). (G and H) Blood glucose levels during IPITTs and quantification of AUC ($n = 5$). (I) Representative ORO-staining images of liver tissues from *db*/*db* mice ($n = 5$). Scale bar: 100 μm. (J and K) ELISA analysis of the expression levels of IL-6 (J) and TNF-α (K) in the liver ($n = 5$). (L and M) Western blot (L) and immunofluorescence analysis (M) of the expression levels of HSP70 in the liver ($n = 5$). Scale bar: 100 μm. (N and O) Western blot (N) and immunofluorescence (O) analysis of the expression levels of *p*-JNK in the liver ($n = 5$). Scale bar: 100 μm. All data are presented as mean ± S.D. Statistical analysis was conducted using one-way ANOVA. *$p \leq 0.05$, **$p \leq 0.01$, ***$p \leq 0.001$ and ****$p \leq 0.0001$.

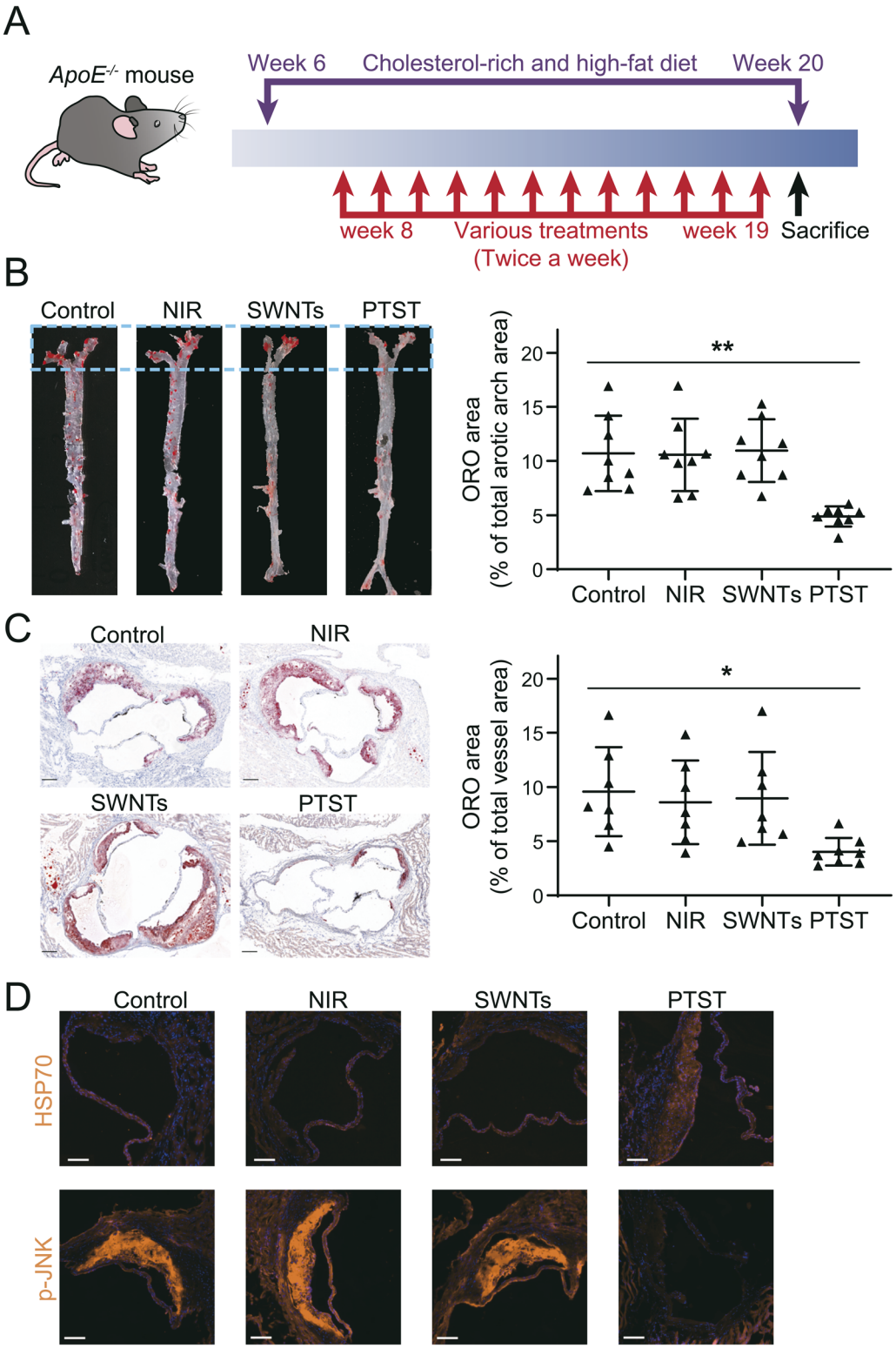

Fig. 7 *In vivo* PTST prevented atherosclerosis. (A) Schematic illustration of *ApoE*$^{-/-}$ mice receiving various treatments. (B) Representative images of ORO-stained aortic sinus sections. Scale bar = 100 μm. Quantification of the ORO-stained area of the aortic sinus is shown on the right ($n = 8$). (C) Representative images of ORO-stained aortic sinus sections. Scale bar: 100 μm. Quantification of the ORO-stained area is shown on the right ($n = 7$). (D) Immunofluorescence analysis of the expression of HSP70 and phosphorylation of JNK ($n = 7$). Scale bar: 50 μm. All data are presented as mean ± SD. Statistical analysis was conducted using one-way ANOVA. *$p \leq 0.05$, **$p \leq 0.01$.

PTST relieves T2D

We successfully demonstrated that PTST could alleviate inflammation *in vitro* and sufficient SWNTs could be accumulated in lesional tissues. Hence, we next explored whether PTST could alleviate inflammation and related diseases *in vivo*. The *db*/*db* mice, T2D model mice, exhibit hyperglycemia associated with obesity at 6 weeks of age. For the therapy of T2D, *db*/*db* mice (male, 6 weeks) were randomly divided into 4 groups: (a) control group; (b) NIR group; (c) SWNTs group; (d) PTST group. WT mice were regarded as healthy controls. The SWNT solution (1 mg kg^{-1}) was administered intravenously in groups (c) and (d) twice a week, while the mice in groups (a) and (b) received the same volume of PBS. 4 hours post injection, groups (b) and (d) were irradiated using NIR (808 nm, 0.5 W cm^{-2}) at the liver site for 25 min (Fig. 6A). At the age of 6 weeks, fasting blood glucose of four groups of *db*/*db* mice was about 10 mmol L^{-1}, which was higher than that of the WT group (about 6 mmol L^{-1}) (Fig. 6B). These data proved that *db*/*db* mice had hyperglycemia symptoms at the age of 6 weeks. Throughout the experimental period (6–10 weeks of age), fasting glucose of the PTST group and WT group remained constant, while the other three groups increased to around 20 mmol L^{-1} (Fig. 6B). After 4 weeks of treatment, the PTST resulted in reduced fasting insulin levels and insulin resistance as measured by the homeostatic model assessment of insulin resistance (HOMA-IR) (Fig. 6C and D). In contrast, *db*/*db* mice of the other three groups suffered from hyperglycemia, hyperinsulinemia, and elevated HOMA-IR (Fig. 6B–D). We also performed intraperitoneal injection (I.P.) glucose tolerance tests (IPGTTs) and I.P. insulin tolerance tests (IPITTs) on the mice. The PTST group showed a markedly improved insulin and glucose tolerance (Fig. 6E–H). Histological evaluation *via* oil red O (ORO) -staining showed that PTST alleviated hepatic steatosis (Fig. 6I). *db*/*db* mice also had symptoms of polydipsia and polyuria. We found that the mouse bedding of the PTST group was drier than that of the other three groups (Fig. S15A), and food and water intake of the PTST group were lower than that of the other three groups (Fig. S15B and C). In conclusion, PTST alleviated a series of symptoms of T2D.

We further explored whether hepatic inflammation was relieved after PTST. According to the ELISA data, the lowest level of inflammatory cytokines in livers was observed in the PTST group (Fig. 6J and K). Furthermore, the expression of HSP70 was downregulated in the livers of *db*/*db* mice compared with that in WT mice. After PTST treatment, the expression of HSP70 in the liver was significantly increased and higher than that of the WT group, while there was no change in the HSP70 level in the NIR and SWNTs groups (Fig. 6L and M). We also tested the level of HSP70 in serum and found that there was no significant difference among all groups (Fig. S16), which indicated PTST did not change eHSP70. In addition, the lowest level of phosphorylation of JNK (Fig. 6N and O) in livers was observed in the PTST group. These data showed that PTST could efficiently upregulate the expression of HSP70 and relieve inflammation *in vivo*. During the experiment, the body weight of mice in each group had no significant difference and continued to increase (Fig. S17). The hematoxylin and eosin (H&E) staining photos of the main organs showed that no obvious damage was observed in each group (Fig. S18). These results verified that it was safe to use SWNTs to implement PTST.

PTST prevents atherosclerosis

To assess the therapeutic effect of PTST on atherosclerosis, *ApoE*$^{-/-}$ mice (male, 8 weeks) on a high-fat diet were randomly divided into 4 groups as described above (control, NIR, SWNT and PTST groups). SWNTs were injected twice a week, and the cardiac region was irradiated to NIR (0.5 W cm^{-2}) for 25 min, 12 hours post injection (Fig. 7A). After 12 weeks of treatment, in the PTST group, ORO-staining displayed a significant 45.8% reduction (4.9% *vs.* 10.7%) in en face prepared aortic arch lesion areas (within the dashed box) and 41% reduction (4.0% *vs.* 9.6%) in aortic sinus areas compared with the control group (Fig. 7B and C). In comparison, no significant change in the lesion aortic arch and sinus areas was observed in the NIR group and the SWNTs group. As shown in Fig. 7D, the increased expression of HSP70 and decreased phosphorylation of JNK in the aortic sinus of the PTST group indicated that PTST prevents inflammation in the aortic arch, which explains the therapeutic effect. The level of HSP70 in serum showed no significant difference between each group (Fig. S19). During the experiment, the body weight of mice in each group had no significant difference and continued to increase (Fig. S20). H&E staining of the main organs shows that obvious damage was observed in each group (Fig. S21). These data verified that PTST was a safe and effective way for treating atherosclerosis.

Conclusions

In conclusion, we developed a universal approach, designated as PTST, for both imaging and treating metaflammation. SWNTs were utilized as targeted vectors to navigate inflamed tissues *via* Ly-6C^{hi} monocyte hitchhiking, leveraging their PA properties to precisely locate the lesional tissues. Our results validated that SWNTs were taken up by almost 100% of Ly-6C^{hi} monocytes in peripheral blood and 40% of lesional macrophages, with the accumulated SWNTs proving to be highly efficient for PA imaging. Together with NIR light, we achieved local and temporal regulation of HSP70 expression in lesional tissues. Upregulation of HSP70 restores the ability of lesional cells to combat inflammatory and metabolic stress, thus alleviating the symptoms of metabolic diseases. PTST harnesses the photothermal effect at cell-tolerable temperatures, utilizing this as a signal to modulate immune cell function rather than inducing cell death. We successfully used SWNTs to identify inflamed liver and aorta and relieved the symptoms of *db*/*db* mice and *ApoE*$^{-/-}$ mice after a period of PA imaging-guided PTST.

Ethical statement

All animal experiments followed relevant laws and were approved by the Institutional Animal Care and Use Committee of Hunan University [protocol number: SYXK (xiang) 2022-

0007]. The experiments were conducted following the guidelines provided by the Guide for the Care and Use of Laboratory Animals.

Author contributions

Ruixi Peng: conceptualization, formal analysis, investigation, visualization and writing – original draft. Mengyun He: methodology and investigation. Yi Yuan: investigation and validation. Li-juan Tang: funding acquisition. Jianhui Jiang: resources. Xia Chu: conceptualization, funding acquisition, resources, supervision and writing – review & editing.

Conflicts of interest

There are no conflicts to declare.

Data availability

Additional data are available from the corresponding author upon reasonable request.

Main experimental data are provided within the main text and the SI. See DOI: **https://doi.org/10.1039/d5sc05091j**.

Acknowledgements

This work was supported by the National Natural Science Foundation of China (No. 21991080, 22374042, and 22374041) and the Science and Technology Major Project of Hunan Province (No. 2021SK1020).

Notes and references

1 G. S. Hotamisligil, Inflammation, metaflammation and immunometabolic disorders, *Nature*, 2017, **542**, 177–185.
2 H. Charles-Messance, K. A. J. Mitchelson, E. De Marco Castro, F. J. Sheedy and H. M. Roche, Regulating metabolic inflammation by nutritional modulation, *J. Allergy Clin. Immunol.*, 2020, **146**, 706–720.
3 M. W. Schleh, H. L. Caslin, J. N. Garcia, M. Mashayekhi, G. Srivastava, A. B. Bradley and A. H. Hasty, Metaflammation in obesity and its therapeutic targeting, *Sci. Transl. Med.*, 2023, **15**, eadf9382.
4 W. Y. Geng, W. Y. Liao, X. Y. Cao and Y. Y. Yang, Therapeutic targets and approaches to manage inflammation of NAFLD, *Biomedicines*, 2025, **13**, 393.
5 T. V. Rohm, D. T. Meier, J. M. Olefsky and M. Y. Donath, Inflammation in obesity, diabetes, and related disorders, *Immunity*, 2022, **55**, 31–55.
6 A. Ajoolabady, D. Pratico, L. Lin, C. S. Mantzoros, S. Bahijri, J. Tuomilehto and J. Ren, Inflammation in atherosclerosis: pathophysiology and mechanisms, *Cell Death Dis.*, 2024, **15**, 817.
7 L. E. Hightower, Heat shock, stress proteins, chaperones, and proteotoxicity, *Cell*, 1991, **66**, 191–197.
8 T. P. Shanley, M. A. Ryan, T. Eaves-Pyles and H. R. Wong, Heat shock inhibits phosphorylation of I-kappa B alpha, *Shock*, 2000, **14**, 447–450.
9 B. J. Grossman, T. P. Shanley, K. Odoms, K. E. Dunsmore, A. G. Denenberg and H. R. Wong, Temporal and mechanistic effects of heat shock on LPS-mediated degradation of I kappa B alpha in macrophages, *Inflammation*, 2002, **26**, 129–137.
10 D. Tang, R. Kang, W. Xiao, H. Wang, S. K. Calderwood and X. Xiao, The anti-inflammatory effects of heat shock protein 72 involve inhibition of high-mobility-group box 1 release and proinflammatory function in macrophages, *J. Immunol.*, 2007, **179**, 1236–1244.
11 U. Brykczynska, M. Geigges, S. J. Wiedemann, E. Dror, M. Boni-Schnetzler, C. Hess, M. Y. Donath and R. Paro, Distinct transcriptional responses across tissue-resident macrophages to short-term and long-term metabolic challenge, *Cell Rep.*, 2020, **30**, 1627–1643.
12 J. Chung, A. K. Nguyen, D. C. Henstridge, A. G. Holmes, M. H. S. Chan, J. L. Mesa, G. I. Lancaster, R. J. Southgate, C. R. Bruce, S. J. Duffy, I. Horvath, R. Mestril, M. J. Watt, P. L. Hooper, B. A. Kingwell, L. Vigh, A. Hevener and M. A. Febbraio, HSP72 protects against obesity-induced insulin resistance, *Proc. Natl. Acad. Sci. U. S. A.*, 2008, **105**, 1739–1744.
13 J. A. Inia and E. R. O'Brien, Role of heat shock protein 27 in modulating atherosclerotic inflammation, *J. Cardiovasc. Transl. Res.*, 2021, **14**, 3–12.
14 Z. W. Nie, C. S. Xiao, Y. Z. Wang, R. K. Li and F. C. Zhao, Heat shock proteins (HSPs) in non-alcoholic fatty liver disease (NAFLD): from molecular mechanisms to therapeutic avenues, *Biomark. Res.*, 2024, **12**, 120.
15 S. M. Gehrig, C. van der Poel, T. A. Sayer, J. D. Schertzer, D. C. Henstridge, J. E. Church, S. Lamon, A. P. Russell, K. E. Davies, M. A. Febbraio and G. S. Lynch, Hsp72 preserves muscle function and slows progression of severe muscular dystrophy, *Nature*, 2012, **484**, 394–398.
16 D. C. Henstridge, C. R. Bruce, B. G. Drew, K. Tory, A. Kolonics, E. Estevez, J. Chung, N. Watson, T. Gardner, R. S. Lee-Young, T. Connor, M. J. Watt, K. Carpenter, M. Hargreaves, S. L. McGee, A. L. Hevener and M. A. Febbraio, Activating HSP72 in rodent skeletal muscle increases mitochondrial number and oxidative capacity and decreases insulin resistance, *Diabetes*, 2014, **63**, 1881–1894.
17 M. Hirunsai and R. Srikuea, Heat stress ameliorates tenotomy-induced inflammation in muscle-specific response *via* regulation of macrophage subtypes, *J. Appl. Physiol.*, 2020, **128**, 612–626.
18 C. Imtiaz, M. A. Farooqi, T. Bhatti, J. Lee, R. Moin, C. U. Kang and H. M. U. Farooqi, Focused Ultrasound, an Emerging Tool for Atherosclerosis Treatment: A Comprehensive Review, *Life*, 2023, **13**, 1783.
19 H. S. Ban, T. S. Han, K. Hur and H. S. Cho, Epigenetic alterations of heat shock proteins (HSPs) in cancer, *Int. J. Mol. Sci.*, 2019, **20**, 16.

20 K. Hayashi, F. Nikolos, Y. C. Lee, A. Jain, E. Tsouko, H. Gao, A. Kasabyan, H. E. Leung, A. Osipov, S. Y. Jung, A. V. Kurtova and K. S. Chan, Tipping the immunostimulatory and inhibitory DAMP balance to harness immunogenic cell death, *Nat. Commun.*, 2020, **11**, 6299.

21 H. A. Amissah, S. E. Combs and M. Shevtsov, Tumor dormancy and reactivation: the role of heat shock proteins, *Cells*, 2024, **13**, 1087.

22 X. Li, J. F. Lovell, J. Yoon and X. Chen, Clinical development and potential of photothermal and photodynamic therapies for cancer, *Nat. Rev. Clin. Oncol.*, 2020, **17**, 657–674.

23 I. C. Miller, A. Zamat, L. K. Sun, H. Phuengkham, A. M. Harris, L. Gamboa, J. Yang, J. P. Murad, S. J. Priceman and G. A. Kwong, Enhanced intratumoural activity of CAR T cells engineered to produce immunomodulators under photothermal control, *Nat. Biomed. Eng.*, 2021, **5**, 1348–1359.

24 W. Gao, Y. H. Sun, M. Cai, Y. J. Zhao, W. H. Cao, Z. H. Liu, G. W. Cui and B. Tang, Copper sulfide nanoparticles as a photothermal switch for TRPV1 signaling to attenuate atherosclerosis, *Nat. Commun.*, 2018, **9**, 231.

25 X. Q. Chen, Q. Y. Yang, W. Y. Kong, Y. F. Ge, J. He, A. Yan and D. Li, High spatial- resolved heat manipulating membrane heterogeneity alters cellular migration and signaling, *Proc. Natl. Acad. Sci. U. S. A.*, 2023, **120**, e2312603120.

26 T. Dai, W. M. He, S. S. Tu, J. R. Han, B. Yuan, C. Y. Yao, W. Z. Ren and A. G. Wu, Black TiO_2 nanoprobe-mediated mild phototherapy reduces intracellular lipid levels in atherosclerotic foam cells *via* cholesterol regulation pathways instead of apoptosis, *Bioact. Mater.*, 2022, **17**, 18–28.

27 J. Sheng, Z. Y. Zu, J. C. Qi, Y. G. Zhang, H. G. Wu, Z. C. Wang, Y. Miao, T. Zheng, S. Wang, L. L. Zhang, G. M. Lu and L. J. Zhang, Mild low-temperature photothermal therapy demonstrated a distinctive 'hot spring' effect in the multichannel regulation of atherosclerosis instead of inducing foam cell apoptosis, *Chem. Eng. J.*, 2024, **485**, 149882.

28 B. R. Smith, E. E. Ghosn, H. Rallapalli, J. A. Prescher, T. Larson, L. A. Herzenberg and S. S. Gambhir, Selective uptake of single-walled carbon nanotubes by circulating monocytes for enhanced tumour delivery, *Nat. Nanotechnol.*, 2014, **9**, 481–487.

29 F. K. Swirski, M. J. Pittet, M. F. Kircher, E. Aikawa, F. A. Jaffer, P. Libby and R. Weissleder, Monocyte accumulation in mouse atherogenesis is progressive and proportional to extent of disease, *Proc. Natl. Acad. Sci. U. S. A.*, 2006, **103**, 10340–10345.

30 M. Gifani, D. J. Eddins, H. Kosuge, Y. P. Zhang, S. L. A. Paluri, T. Larson, N. Leeper, L. A. Herzenberg, S. S. Gambhir, M. V. McConnell, E. E. B. Ghosn and B. R. Smith, Ultraselective carbon nanotubes for photoacoustic imaging of inflamed atherosclerotic plaques, *Adv. Funct. Mater.*, 2021, **31**, 2101005.

31 H. M. Li, P. J. Li, J. R. Zhang, Z. Y. Lin, L. T. Bai and H. Y. Shen, Applications of nanotheranostics in the second near-infrared window in bioimaging and cancer treatment, *Nanoscale*, 2024, **16**, 21697–21730.

32 Y. Ma, W. Sun, Z. F. Ye, L. H. Liu, M. H. Li, J. H. Shang, X. Y. Xu, H. Cao, L. Xu, Y. C. Liu, X. Q. Kong, G. S. Song and X. B. Zhang, Oxidative stress biomarker triggered multiplexed tool for auxiliary diagnosis of atherosclerosis, *Sci. Adv.*, 2023, **9**, 19.

33 P. Lu, S. M. Dai, H. H. Zhou, F. L. Wang, W. R. Dong and J. H. Jiang, Xanthene-based near-infrared chromophores for high-contrast fluorescence and photoacoustic imaging of dipeptidyl peptidase 4, *Chem. Sci.*, 2024, **15**, 2221–2228.

34 A. M. Flores, N. Hosseini-Nassab, K. U. Jarr, J. Q. Ye, X. J. Zhu, R. Wirka, A. L. Koh, P. Tsantilas, Y. Wang, V. Nanda, Y. Kojima, Y. T. Zeng, M. Lotfi, R. Sinclair, I. L. Weissman, E. Ingelsson, B. R. Smith and N. J. Leeper, Pro-efferocytic nanoparticles are specifically taken up by lesional macrophages and prevent atherosclerosis, *Nat. Nanotechnol.*, 2020, **15**, 154–161.

35 Z. Liu, S. M. Tabakman, Z. Chen and H. Dai, Preparation of carbon nanotube bioconjugates for biomedical applications, *Nat. Protoc.*, 2009, **4**, 1372–1381.

36 G. C. Ma, Q. H. Ding, Y. Wang, Z. W. Zhang, Y. D. Zhang, H. Shi, L. T. Cai, P. Gong, P. F. Zhang, Z. Cheng and J. S. Kim, Precision photothermal therapy at mild temperature: NIR-II imaging-guided, H_2O_2-responsive stealth nanobomb, *Adv. Healthcare Mater.*, 2024, **13**, e2400514.

37 L. Gamboa, E. V. Phung, H. X. Li, J. P. Meyers, A. C. Hart, I. C. Miller and G. A. Kwong, Heat-triggered remote control of CRISPR-dCas9 for tunable transcriptional modulation, *ACS Chem. Biol.*, 2020, **15**, 533–542.

38 S.-I. Yamaguchi, Q. Xie, F. Ito, K. Terao, Y. Kato, M. Kuroiwa, S. Omori, H. Taniura, K. Kinoshita, T. Takahashi, S. Toyokuni, K. Kasahara and M. Nakayama, Carbon nanotube recognition by human Siglec-14 provokes inflammation, *Nat. Nanotechnol.*, 2023, **18**, 628–636.

39 Q. Liu, S. F. Li, D. Ma, J. R. Chen, C. M. Li, W. H. Zhuang and M. Chen, Ros-responsive nano-platform for lipid-specific fluorescence imaging of atherosclerosis, *J. Colloid Interface Sci.*, 2024, **667**, 520–528.

40 W. Gao, L. J. Lv, G. H. Li, H. X. Zhao, J. Zhou, Y. Cheng and B. Tang, Multi-effective nanoplatform with down/upconversion dual-mode emissions for NIR-II imaging and PDT/PTT synergistic therapy of early atherosclerosis, *Chem. Commun.*, 2024, **60**, 10386–10389.

41 H. Yang, T. T. Yang, C. Heng, Y. Zhou, Z. Z. Jiang, X. Qian, L. Du, S. Y. Mao, X. X. Yin and Q. Lu, Quercetin improves nonalcoholic fatty liver by ameliorating inflammation, oxidative stress, and lipid metabolism in *db*/*db* mice, *Phytother. Res.*, 2019, **33**, 3140–3152.